EARTHQUAKE ENGINEERING AND STRUCTURAL DYNAMICS
Earthquake Engng Struct. Dyn. 2000; **29**:63–83

Modelling non-linear ground response of non-liquefiable soils

Ronaldo I. Borja*,†, Chao-Hua Lin‡, Kossi M. Sama‡ and Gwynn M. Masada‡

Department of Civil and Environmental Engineering, Stanford University, Stanford, CA 94305-4020, U.S.A.

SUMMARY

A non-linear finite element (FE) model is presented to account for soil column effects on strong ground motion. A three-dimensional bounding surface plasticity model with a vanishing elastic region, appropriate for non-liquefiable soils, is formulated to accommodate the effects of plastic deformation right at the onset of loading. The elasto-plastic constitutive model is cast within the framework of a FE soil column model, and is used to re-analyse the downhole motion recorded by an array at a Large-Scale Seismic Test (LSST) site in Lotung, Taiwan, during the earthquake of 20 May 1986; as well as the ground motion recorded at Gilroy 2 reference site during the Loma Prieta earthquake of 17 October 1989. Results of the analysis show maximum permanent shearing strains experienced by the soil column in the order of 0.15 per cent for the Lotung event and 0.8 per cent for the Loma Prieta earthquake, which correspond to modulus reduction factors of about 30 and 10 per cent respectively, implying strong non-linear response of the soil deposit at the two sites. Copyright © 2000 John Wiley & Sons, Ltd.

KEY WORDS: ground response; site amplification; soil plasticity; soil-structure interaction

1. INTRODUCTION

It is generally recognized that soils exhibit non-linear behaviour under shear loading conditions. Shear modulus decreases with increasing strain with an accompanying increase in material damping [1]. These changes in material properties control the amplitude and frequency content of computed ground motions, and must be accommodated in the non-linear constitutive relations to realistically model the ground response.

In general, two approaches are conventionally used to model non-linear cyclic soil stress–strain behaviour: equivalent linear and truly non-linear [2]. The equivalent linear approach approximates

*Correspondence to: Ronaldo I. Borja, Department of Civil and Environmental Engineering, Stanford University, Stanford, CA 94305-4020, U.S.A.
†Associate Professor.
‡Graduate Student.

Contract/grant sponsor: Earthquake Hazard Mitigation Division of National Science Foundation; contract/grant numbers: CMS-9114869 and CMS-9613906.

Received 21 April 1998
Revised 22 June 1999
Accepted 22 August 1999

CCC 0098–8847/2000/010063–21$17.50

a second-order non-linear equation by a linear equation expressed in terms of an effective shear strain [3]. This approach has the advantage of mathematical simplicity and the preservation of the principle of superposition, but has the disadvantage of giving poor predictions at large strains and inability to model plastic deformation and/or failure. The program SHAKE [4] is the most widely used analysis package to perform one-dimensional site response calculations using the equivalent linear approach.

Non-linear approaches, on the other hand, utilize either the finite element scheme [5], finite difference scheme [6], or the method of characteristics [7], to solve the wave propagation problem. An important element of non-linear approaches is a non-linear model that characterizes the cyclic mechanical soil response. Nonlinear soil models commonly utilized in dynamic analyses include the Ramberg–Osgood model, the hyperbolic model, the Davidenkov model, and many other elasto-plastic models that have varying degrees of complexities [2]. One-dimensional non-linear soil models such as the first three models mentioned above have limited use in that they rely on the assumption of planar waves.

This paper presents a three-dimensional bounding surface plasticity model with a vanishing elastic region capable of capturing the essential features of many one-dimensional non-linear soil models. The constitutive model is reformulated from a version presented previously by Borja and Amies [8], derived from the idea of Dafalias and Popov [9], and includes provisions for the translation of the bounding surface and decomposition of the response into inviscid and viscous parts. The model is formulated in terms of total stresses, and hence is appropriate for non-liquefiable soils such as partially saturated soils and clays. An important attribute of the proposed model is that it only requires the moduli ratio-shear strain degradation curve and the zero-strain asymptote of the damping ratio curve, in addition to the usual shear and compressional wave velocity profiles, to completely characterize the soil deposit.

The elasto-plastic constitutive model is cast within the framework of a FE soil column model and used to re-analyze the downhole motion recorded by an array at a Large-Scale Seismic Test (LSST) site in Lotung, Taiwan, during the earthquake of 20 May 1986 (known in the literature as the LSST7 event), as well as the ground motion recorded at Gilroy 2 site during the Loma Prieta earthquake of 17 October 1989. The Gilroy 2 site is characterized by a deep water table, and pore pressure build-up and liquefaction are not of major concern, so the model is appropriate for this case study. As for the Lotung test site, pore pressure sensors were not yet available at the time of the LSST7 event, but there was no documentation of liquefaction at the site during this event. While it is likely that excess pore pressures did build up during the LSST7 event based on observations made from later events [10] (such as the earthquakes of July and November of 1986), no attempt was made in the present work to include the effect of pore pressure build-up in the simulations.

Some models are arguably more robust than the one presented in this paper; however, in general, they require numerous parameters that are difficult to determine accurately in practice. Furthermore, they tend to be quite sensitive to the chosen values of the material parameters [11]. The latter point is crucial since even the simplest form of non-linear material characterization, the degradation of shear moduli with shear strain, can be difficult to establish accurately in practice unless one performs very careful laboratory experiments [12]. Considering that there is a large variation in the amount of site-specific information available for estimating ground motion at a site, it is important to start with a simple enough non-linear soil model such as the one advocated in this paper.

2. OVERVIEW OF NON-LINEAR GROUND RESPONSE MODEL

The ground response model advocated in this paper is a module of a non-linear structure dynamics finite element (FE) code named SPECTRA [13, 14]. This code is written in Fortran 90 and contains column elements, called 'sticks', for vertical wave propagation analysis. Stick elements can accommodate general non-planar waves, and have no rocking mode. The displacement field is interpolated bilinearly, and the solution is integrated in time domain via the alpha-method [15].

SPECTRA has a material module that accommodates three-dimensional deformation and formulated within the framework of bounding surface plasticity with a vanishing elastic region [8]. Central to the formulation of the constitutive model is the assumption of an additive decomposition of the Cauchy stress tensor $\boldsymbol{\sigma}$ into inviscid and viscous components,

$$\boldsymbol{\sigma} = \boldsymbol{\sigma}^{\text{inv}} + \boldsymbol{\sigma}^{\text{vis}} \tag{1}$$

Specific forms for $\boldsymbol{\sigma}^{\text{inv}}$ and $\boldsymbol{\sigma}^{\text{vis}}$ are

$$\boldsymbol{\sigma}^{\text{inv}} = \boldsymbol{c}^{\text{e}} : (\boldsymbol{\varepsilon} - \boldsymbol{\varepsilon}^{\text{p}}); \quad \boldsymbol{\sigma}^{\text{vis}} = \boldsymbol{d} : \dot{\boldsymbol{\varepsilon}} \tag{2}$$

where $\boldsymbol{c}^{\text{e}}$ is the rank-four elastic moduli tensor, $\boldsymbol{\varepsilon}$ is the symmetric small strain tensor, $\boldsymbol{\varepsilon}^{\text{p}}$ is the plastic component of $\boldsymbol{\varepsilon}$, $\boldsymbol{d}$ is the rank-four material viscous damping tensor, $\dot{\boldsymbol{\varepsilon}}$ is the first time derivative of $\boldsymbol{\varepsilon}$, and the symbol ':' denotes a tensor contraction.

Assuming isotropy in the material response, the tensors $\boldsymbol{c}^{\text{e}}$ and $\boldsymbol{d}$ can be expressed in terms of the bulk and shear moduli, K^{e} and G^{e}, and the bulk and shear damping coefficients, $\mathscr{K}$ and $\mathscr{G}$, respectively. The special case where $K^{\text{e}}/G^{\text{e}} = \mathscr{K}/\mathscr{G}$ leads to a viscous damping tensor $\boldsymbol{d}$ that is linearly proportional to the elastic moduli tensor $\boldsymbol{c}^{\text{e}}$ through a relationship of the form

$$\boldsymbol{d} = \chi \boldsymbol{c}^{\text{e}}; \quad \chi = 2\xi_0/\omega \tag{3}$$

where ξ_0 is the value of damping ratio in the limit of zero shear strain (see Reference [1]), and ω is the angular frequency of the motion. The theory thus relies on the hypothesis of a nonzero asymptote of the damping ratio curve in the limit of zero strain, otherwise, there will be no viscous damping. Indeed, experimental evidence suggests that the damping ratio is really never zero due to energy dissipation even at very low strain levels [2].

The inviscid component of the constitutive model is based on a three-dimensional J_2-type bounding surface plasticity theory with a vanishing elastic region proposed in Borja and Amies [8]. Recently, this model has been enhanced to allow the bounding surface to translate in the stress space, and thus, capture hardening/softening of shear strength with loading as well as provide a more stable numerical integration algorithm for the hardening case [13, 14]. The translation of the bounding surface is facilitated by interpolating the hardening modulus H' from the exponential function

$$H' = h\kappa^m + H_0 \tag{4}$$

where h and m are the exponential parameters of the model. The dimensionless scalar quantity κ satisfies the condition

$$\| \boldsymbol{\sigma}' + \kappa(\boldsymbol{\sigma}' - \boldsymbol{\sigma}'_0) \| = R \tag{5}$$

where R is the radius of the bounding surface. For the case $H_0 > 0$, the bounding surface hardens kinematically. See Reference [8] for notation and further details of the model.

Figure 1 shows a schematic representation of the model for the case of cyclic simple shear loading. Here, the stress path is a radial line perpendicular to one of three principal stress axes on the π-plane. The stress point τ and the unloading point τ_0 are co-radial on the π-plane, and so we can use this feature to develop an expression for the moduli ratio degradation curve. For cyclic simple shear stress condition without viscous damping, the moduli ratio can be expressed in the form

$$\theta = 1 - \frac{3}{2\gamma_0}\int_0^{2\theta G^e\gamma_0}\left[h\left(\frac{R/\sqrt{2}+\theta G^e\gamma_0-\tau}{\tau}\right)^m + H_0\right]^{-1} d\tau \tag{6}$$

where $\theta = \bar{G}/G^e$ is the moduli ratio, and $\bar{G} = \tau_0/\gamma_0$ is the secant shear modulus (see Figure 1). Equation (6) thus provides a functional relationship between the strain amplitude γ_0 and the moduli ratio θ. In the limit of elastic response, $\gamma_0 \to 0$ and $\theta \to 1$.

Equation (6) can also be used to approximate the backbone curve, assuming that this curve passes through the point $\pm(\gamma_0, \tau_0)$ defined by the hysteresis loop. The backbone curve is given by the expression

$$\tau_0 = \theta G^e \gamma_0 \tag{7}$$

Since $\tau_0 \to \tau_{max}$, where τ_{max} is the maximum shear stress, we can evaluate the value of R as $R = \sqrt{2}\tau_{max}$ (see Figure 1). For practical purposes the value of R (as well as H_0) may be estimated at a finite value of shear strain, say, at $\gamma_0 = 1$ per cent. Furthermore, by choosing appropriate values of h and m, Equation (6) can be made to pass through at least two points on the actual moduli ratio degradation curve for given values of R, H_0 and G^e. Sections 3 and 4 illustrate this procedure for determining the material parameters used for the Lotung LSST and Gilroy 2 case studies.

Figure 2 shows the implications of decomposing the stresses additively into inviscid and viscous parts within the context of simple shear loading. As depicted in Figure 2(a), incorporating the viscous effect provides for a smoother transition of the stress–strain curve on reverse loading. In contrast, the inviscid response (dashed curve) shows a sharp corner at the unloading point. At any stage of loading the area of the hysteresis loop is the sum of the area due to (inviscid)

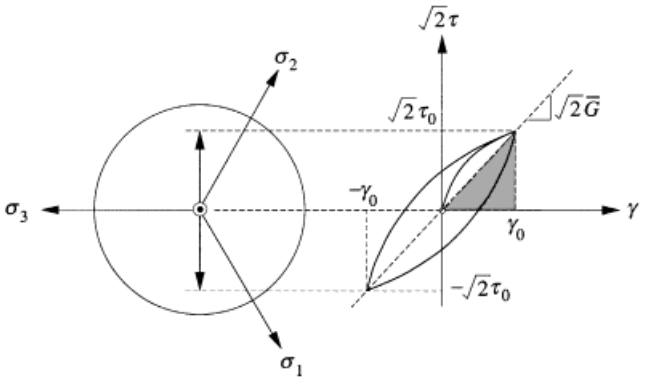

Figure 1. Hysteretic damping in soils subjected to cyclic simple shear.

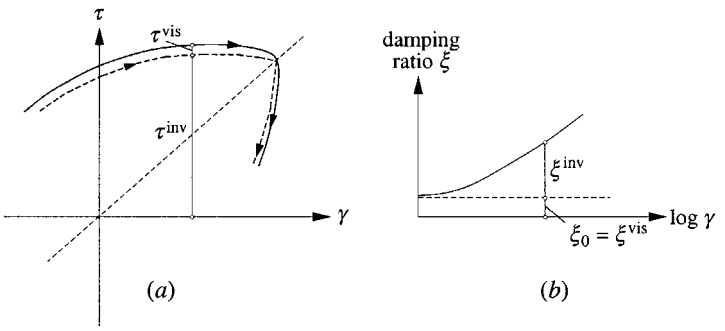

Figure 2. Implications of additive decomposition of stress: (a) load-unload stress-strain curve; (b) damping ratio curve.

hysteretic damping and the area due to viscous damping, as portrayed in Figure 2(b). Since viscous damping is assumed to be independent of the strain level, plastic hysteretic damping becomes more dominant at higher values of shear strain.

3. RE-ANALYSIS OF GROUND RESPONSE AT LOTUNG TEST SITE

Lotung is a seismically active region in northeastern Taiwan, and was the site of two scaled-down nuclear plant containment structures (1/4-scale and 1/12-scale models) constructed by Electric Power Research Institute, in cooperation with Taiwan Power Company, for soil–structure interaction research [16]. The site contains surface and downhole free-field instrumentation in a Large-Scale Seismic Test (LSST) array. On 20 May 1986, a strong earthquake, denoted as the LSST7 event, with magnitude 6.5, epicentral distance of 66 km, and focal depth of 15.8 km shook the test site. Two downhole arrays located approximately at 3 and 49 m from the edge of the 1/4-scale model (DHA and DHB arrays, respectively), recorded the downhole motions at depths of 0, 6, 11, 17, and 47 m. Borja *et al.* [13, 14] have analysed the downhole motions recorded by both DHA and DHB arrays using the SPECTRA program. This section studies the sensitivity of the results reported in Reference [13] to expected variations in the moduli ratio curves.

A series of geophysical seismic tests were performed to measure shear and compression wave velocities at the LSST site [17]. Figure 3(a) shows the average shear and compressional wave velocity profiles at the site. The shear wave velocity begins at about 100 m/s at the ground surface and reaches a value of about 300 m/s at 60 m depth; the compressional wave velocity, on the other hand, begins at about 300 m/s near the ground surface and increases somewhat linearly to about 1500 m/s at a depth of 10 m, after which it remains essentially constant. Using measured total unit weights of 19.0 kN/m^3 for the sandy/silty/clayey layer and 19.5 kN/m^3 for the more gravelly layer, an undegraded shear modulus profile was developed from the shear wave velocity profile as shown in Figure 3(b). Combining the shear and compression wave velocity profiles gives a value of elastic Poisson's ratio of 0.48 (approximately) for the entire soil profile.

Moduli ratio and damping ratio curves were also developed from laboratory testing of the soil samples [17]. However, in this paper we adopt the moduli ratio response curves developed by Zeghal *et al.* [18] based on the in situ recorded seismic response at the LSST site. The technique

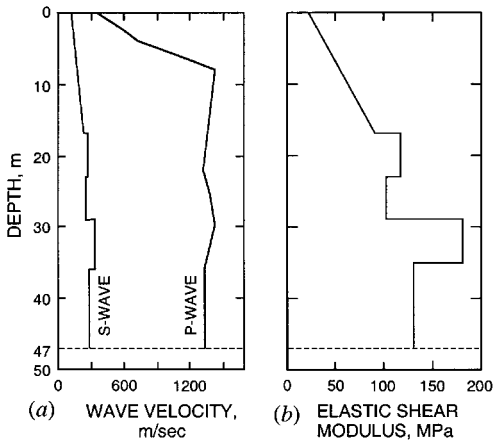

Figure 3. Geophysical testing of soils at Lotung LSST site: (a) wave velocity profile; (b) elastic shear modulus profile.

described in Reference [18] for developing moduli ratio curves eliminates the effects of sample disturbance and uncertainties in laboratory testing, and is generally accurate in the low-strain range (< 0.05 per cent shear strain). A compilation of shear moduli and damping ratios at elevations 6, 11, and 17 m depth from LSST7, LSST12 and LSST16 events is shown in Figure 4, along with representative least-squares best fits as well as upper and lower bounds describing possible variations in the material properties. In using Figure 4 for the simulations, separate curves were assumed for depths of 0–6, 6–11, and 11–17 m. Because data were only available to a depth of 17 m, the soil properties from 17–47 m depth were assumed to be the same as those from 11–17 m depth.

The radius of the bounding surface is computed as $R = \sqrt{2}\tau_{\max}$, where $\tau_{\max}$ is estimated from the moduli ratio curve of Zeghal *et al.* at a shear strain of 5 per cent. This yields $R \approx 0.0015G^{\mathrm{e}}$ and $H_0 \approx 0$. The parameters h and m were then determined such that Equation (6) passes through the in situ moduli degradation curve at moduli ratio values of 0.9 and 0.5, yielding $h \approx 0.63G^{\mathrm{e}}$ and $m \approx 0.97$ for the statistical fit; $h \approx 0.70G^{\mathrm{e}}$ and $m \approx 1.15$ for the upper bound curve; and $h \approx 0.45G^{\mathrm{e}}$ and $m \approx 0.83$ for the lower bound curve. The physical significance of the exponential parameters h and m is described in Figures 5 and 6 of Reference [8] (note the typographical error in Figure 6 of Reference [8], which had the legend for m reversed, i.e. m should be decreasing from 8.0 to 0.5, and not increasing from 0.5 to 8.0). Note that SPECTRA does not use the damping ratio curves, and hence is not affected by the statistical variations in the values of the damping ratio.

As for viscous damping, the zero-strain asymptotes of the damping ratio curves developed in Reference [18] indicate that $\xi_0 = 1$ per cent for the soil at the LSST site. Furthermore, it was shown in Reference [13] that the Fourier transform of the input motion for the LSST7 earthquake had a dominant frequency of $f = 0.65$ Hz (or $\omega = 2\pi f = 4$ rad/s). Using these values, the damping coefficient χ in Equation (3) was estimated to be equal to 0.005 s.

The FE mesh used for the Lotung problem is the same as that used in Reference [13], i.e. 47 stick elements 1 m thick and subjected to seismic excitation at the bottom node. An accuracy analysis of this mesh has been reported in Reference [14] and will not be repeated here. The analysis, which involves eigenvalue studies similar to what will be reported later for the Gilroy 2

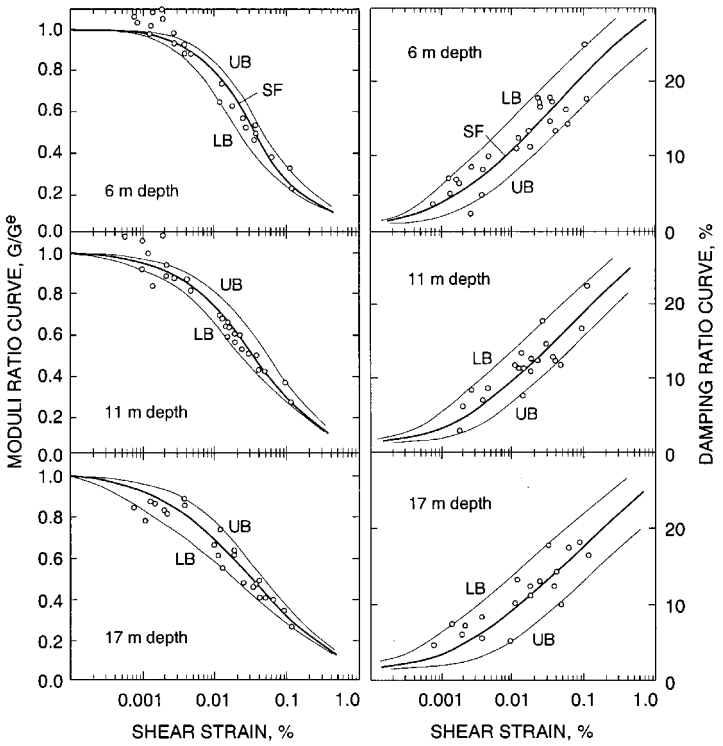

Figure 4. Moduli ratio and damping ratio curves for LSST case study: UB = upper bound; SF = statistical fit; LB = lower bound.

problem, suggests that the mesh can capture the significant frequency contents of the input ground motion.

We now apply simultaneously the three components of the input ground motion, East–West (EW), North–South (NS), and up-down (UD), at the bottom of the FE mesh, and perform a non-linear time-domain analysis. Figures 5 and 6 compare the horizontal ground surface acceleration-time histories predicted by SPECTRA to the ground surface motions recorded by the downhole array DHB. The label FA1-5 was used in the original digitized recording and pertains to the accelerometer installed at the ground surface. The 'bedrock' was assumed to be at a depth of 47 m, where the recorded motion was taken as the input excitation. The predictions were obtained using the same values of the time-integration parameters used previously in Reference [13]: $\beta = 0.3025$, $\gamma = 0.60$, and $\alpha = -0.10$; the time increment was taken as $\Delta t = 0.02$ s.

Results of Figures 5 and 6 show that peak accelerations are predicted by SPECTRA to within 10–20 per cent error in both EW and NS directions if the statistical fit (SF) curve is used to describe the moduli ratio degradation; zero crossings also are predicted quite well. As expected, the model underpredicts the peak values in both directions when lower bound (LB) curves are used for the moduli ratios (see Figure 4). However, the peak values in both directions remain essentially unchanged when upper bound (UB) curves for the data points are used in the

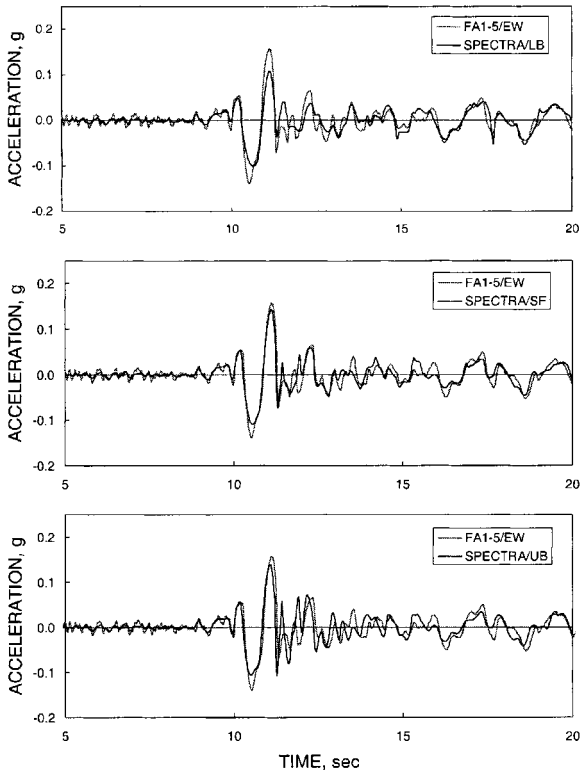

Figure 5. East–West ground surface acceleration-time history using SPECTRA Lotung LSST7 case study.

simulations, although the use of the upper bound curves results in a slight amplification of the secondary peak values.

Figure 7 shows a comparison of observed and predicted resolved horizontal accelerations demonstrating the capability of the model to accommodate the case of vertically propagating non-planar waves (the validity of the assumption of vertically propagating waves is justified by a previous study indicating that the incidence angle of *S*-waves is approximately 6 degrees from the vertical during the LSST7 event [19]). The predictions shown in Figure 7 pertain to the statistical fit curve, and are nearly the same as those reported in Reference [13] using a slightly different set of material parameters. The parameters used in Reference [13] ($H_0 \approx 0.1G^e$, $R \approx 0.001G^e$, $h \approx 1.2G^e$ and $m \approx 0.7$) simply allow the bounding surface to translate in stress space, but essentially capture the statistical fit moduli ratio curve as well. Thus, the model predictions do not depend on the values of the material parameters per se, but on how well these parameters capture the moduli ratio curves for the soil in question.

To compare the performance of SPECTRA with other ground response analysis codes, we repeat the same analysis using SHAKE and again perform a sensitivity study. EW and NS time histories were prescribed separately at a depth of 47 m and the corresponding acceleration-time histories were predicted on the ground surface. Statistical fit, upper bound, and lower bound

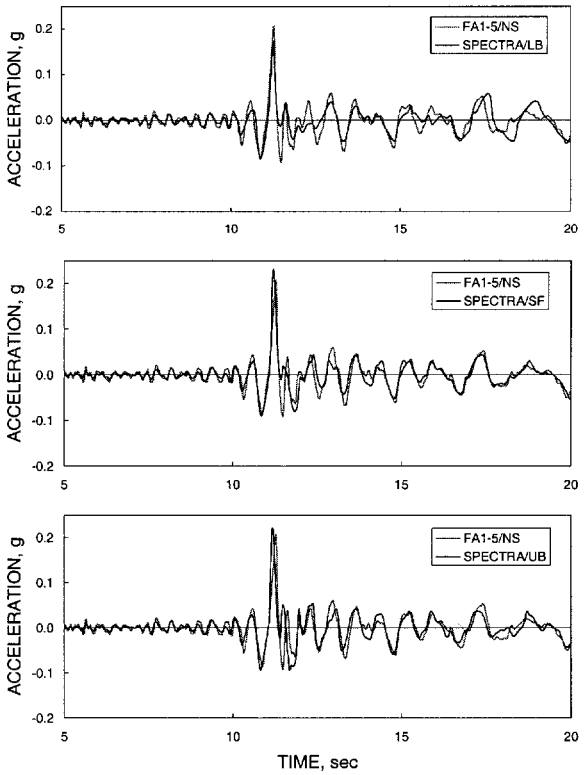

Figure 6. North–South ground surface acceleration-time history using SPECTRA: Lotung LSST7 case study.

shear modulus and damping ratio curves were generated into three separate SHAKE input files, point by point. Values corresponding to shear strain percentages of 0.0001, 0.00025, 0.001, 0.0025, 0.01, 0.025, 0.1, 0.25, and 1.0 for both shear modulus and damping ratio values were input based on the curves shown in Figure 4. The results of the analyses are shown in Figures 8 and 9.

Figures 8 and 9 show that SHAKE predicts the EW motion very well, particularly with the statistical fit curve, but underpredicts the peak NS acceleration quite significantly even with the use of the UB curves. An evident trend exhibited by the SHAKE solutions is that peak values increase monotonically with LB, SF, and UB approximations, in contrast with the trend exhibited by the SPECTRA solutions, which exhibit a 'saturation point' where the SF and UB approximations do not seem to affect the peak values but instead appear to only influence the secondary peaks in both EW and NS directions. Of course, these contrasting trends can be attributed to the fact that SPECTRA is a truly non-linear model whereas SHAKE is only an equivalent linear model.

To further gain an insight into the performance of SPECTRA relative to that of other ground response analysis codes, Figure 10 shows a compilation of the NS ground surface accelerations predicted by three other codes for the LSST7 event, as reported in Reference [20]. The codes considered were DESRA [21], SUMDES [22] and TESS [23], which all used the same recordings at 47 m depth as control motions. The predicted time histories have been generated by

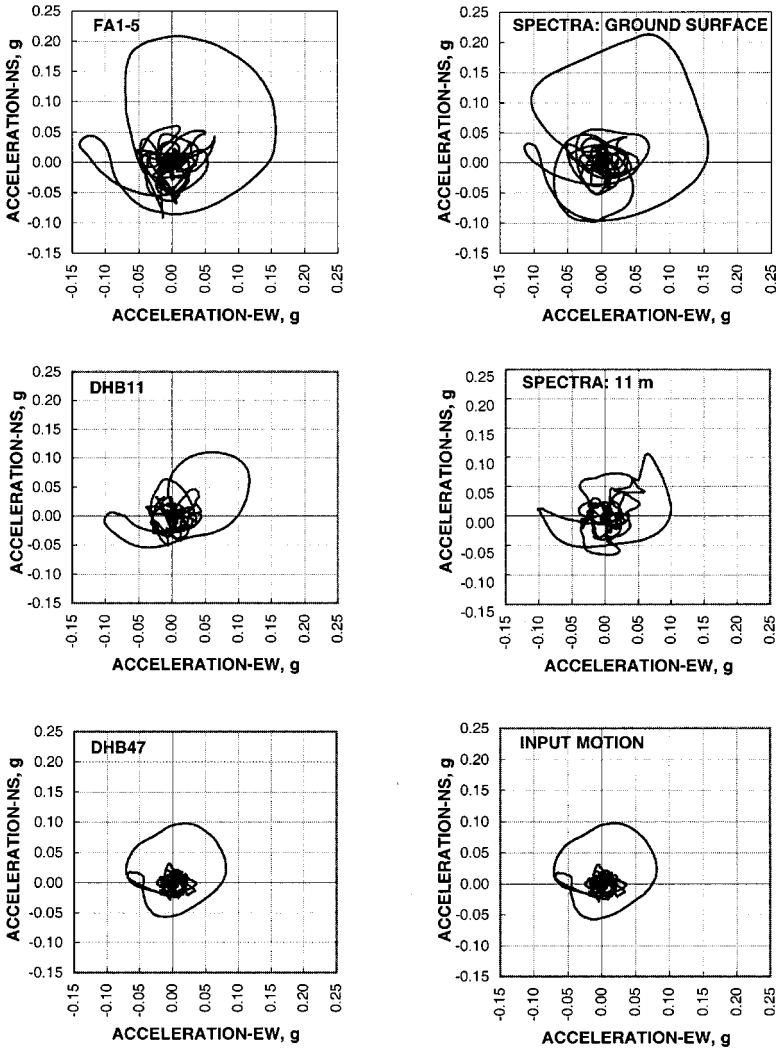

Figure 7. Resolved downhole horizontal acceleration using SPECTRA: Lotung LSST7 case study.

the authors of the codes themselves, reported in and reproduced from Reference [20], and superimposed with the recorded time histories in Figure 10. As shown in Figure 10, all three codes underpredicted the peak values quite substantially, like SHAKE did, even though they were based on moduli ratio and damping ratio curves that are closer to the UB approximations of Figure 4. For comparison purposes, the recorded NS peak acceleration is $0.207g$, whereas the codes considered predicted the following peak values: SPECTRA/LB $= 0.174g$; SPECTRA/SF $= 0.231g$; SPECTRA/UB $= 0.222g$; SHAKE/LB $= 0.124g$; SHAKE/SF $= 0.136g$; SHAKE/UB $= 0.154g$; DESRA $= 0.116g$; SUMDES $= 0.146g$; and TESS $= 0.131g$. Note that the peak for SPECTRA/UB is less than the peak for SPECTRA/SF.

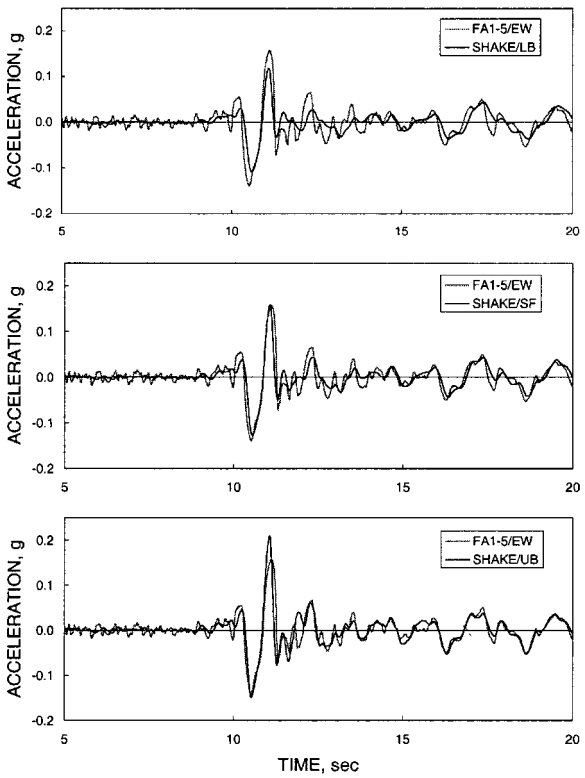

Figure 8. East–West ground surface acceleration-time history using SHAKE: Lotung LSST7 case study.

Figure 11 shows a time-history of the maximum resolved shear strain developed over the 47-m thick soil deposit as predicted by SPECTRA/SF. The maximum shear strain is calculated by computing at each time instant the resolved EW and NS displacements at each nodal point, subtracting the resolved displacements of adjacent nodes to get the relative resolved displacements for each column element, and then dividing them by the element thickness (1 m) to get the resolved shear strain. The element with the largest resolved shear strain is then identified, and this strain is plotted with time. The normal and semi-logarithmic plots of Figure 11 facilitate a clear representation of large- and small-amplitude shear strains. Observe that the maximum resolved shear strain is zero during the first 1.5 s when only *P*-waves have been recorded.

The maximum strain history plot depicted in Figure 11 indicates a peak value of 0.23 per cent coinciding with the arrival of the peak ground acceleration, tapering off to a permanent shear strain value of about 0.12 per cent. Thus, plastic deformation continues to accumulate beyond the arrival of the peak waves, but most of these deformations developed during the period of strongest ground shaking. Reference to the moduli ratio curves of Figure 4 suggests that the secant shear modulus at the point of maximum deformation is around 30 per cent of the elastic value, which implies that the bounding surface was not reached during the course of the solution. This explains the lack of sensitivity of the predictions to the values of R and H_0. At the same point of maximum shear strain the total damping ratio is in the order of about 20 per cent, which is well

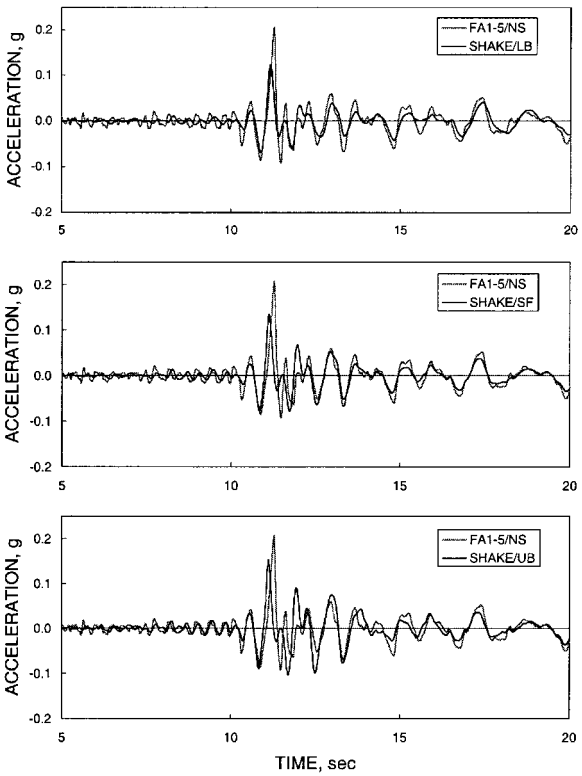

Figure 9. North–South ground surface acceleration-time history using SHAKE: Lotung LSST7 case study.

above the 1 per cent damping ratio used to represent viscous damping. Thus, we can conclude that energy dissipation during the LSST7 event was due primarily to plastic hysteretic damping.

As mentioned previously, pore pressure sensors had not been installed early enough for the LSST7 event, and hence no pore pressure data were available for this event. However, an earthquake of comparable magnitude occurred at the same site on 14 November 1986, denoted as the LSST16 event (magnitude = 7.0, epicentral distance = 78 km, focal depth = 6.9 km), in which pore pressure data have been recorded [24, 25]. As described in Reference [24], the LSST16 event generated excess pore pressure ratios (ratio between excess pore pressure to initial effective vertical stress) in the order of about 25 per cent. Assuming a comparable magnitude for the LSST7 event, these excess pore pressures are sufficiently low to cause significant degradation of soil shear strength and stiffness.

4. GROUND RESPONSE AT GILROY 2 SITE

The second case study involves the Gilroy 2 ground motions from the magnitude 6.9 Loma Prieta earthquake of 17 October 1989. Here, the control motions were taken from the rock site Gilroy 1 located about 2 km west of Gilroy 2. The soil at Gilroy 2 is about 170 m deep and consists of

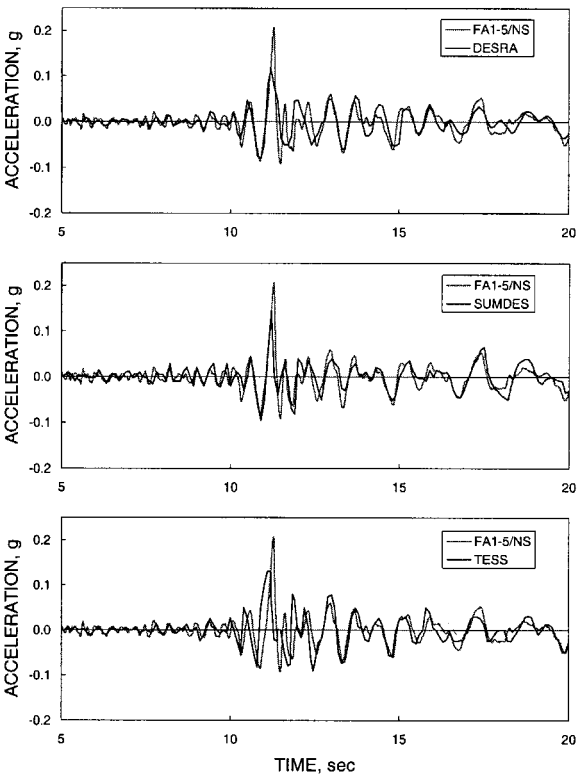

Figure 10. North–South ground surface acceleration-time history using DESRA, SUMDES and TESS: Lotung LSST7 case study (after Reference [20]).

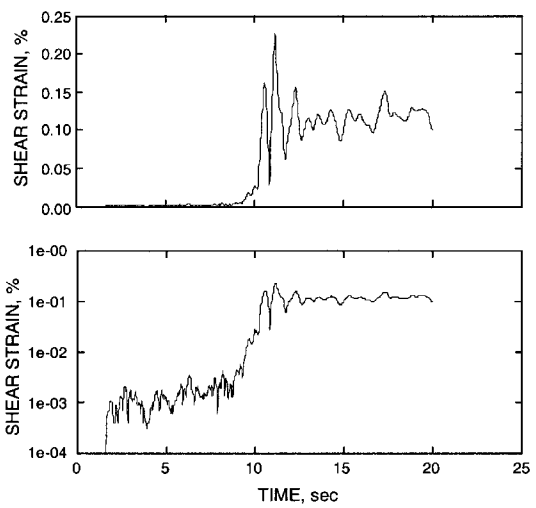

Figure 11. Normal and semi-logarithmic plots of time history of maximum shear strain using SPECTRA: Lotung LSST7 case study.

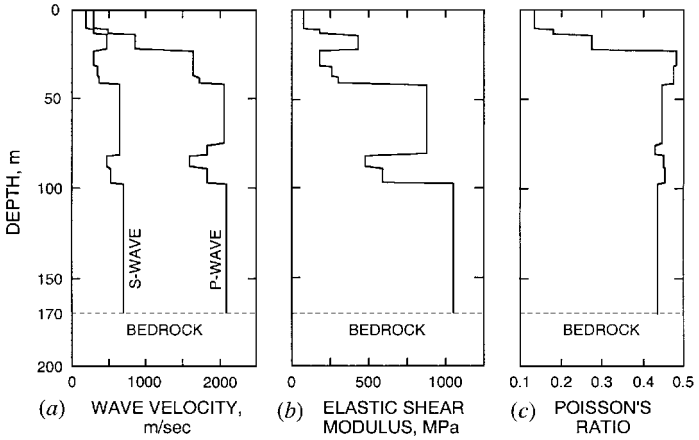

Figure 12. Geophysical testing of soils at Gilroy 2 site: (a) wave velocity profile; (b) elastic shear modulus profile; (c) Poisson's ratio profile.

sands and clays up to a depth of 40 m. Beyond 40 m is a deposit of gravel underlain by weathered bedrock at a depth of about 170 m Gilroy 2 is on the edge of a steeply dipping bedrock interface where two-dimensional basin effects are predicted to be most pronounced [26].

A series of geophysical surveys also were performed to measure shear and compression wave velocities at Gilroy 2 site [20]. Figure 12(a) shows the average shear and compressional wave velocity profiles at the site. The shear wave velocity begins at about 200 m/s at the ground surface and reaches a value of about 700 m/s at 170 m depth; the compressional wave velocity, on the other hand, begins at about 300 m/s and reaches a maximum of about 2100 m/s at a depth of 170 m. Nine undisturbed samples from depths ranging from 3 to 128 m were taken from this site for laboratory testing. For the upper 32 m thick soil layer, the total unit weights of the soil samples are in the order of about 18.8 kN/m^3; below this depth the total unit weights are in the order of 20.9 kN/m^3. Based on the measured unit weights of the soil samples the elastic shear modulus and Poisson's ratio profiles for the site were constructed as shown in Figures 12(b) and (c). For the soil above the water table (situated at depth of 24 m), the values of Poisson's ratio vary from 0.13 to 0.28; below the water table the values range from 0.43 to 0.48, reflecting the influence of saturation.

Moduli ratio and damping curves also were developed from laboratory testing of the soil samples, and the results for the moduli ratio are shown in Figure 13 (see Reference [20]). A total of four moduli ratio curves were developed for the site, representing depths of 0–12; 12–24; 24–40 m; and depths greater than 40 m. Note that the lower modulus reduction at greater depths is due to the presence of gravels below 40 m. From these curves, the radius R of the bounding surface is computed as $R = \sqrt{2}\tau_{\max}$, where $\tau_{\max}$ is obtained from the moduli ratio curves at a shear strain of 5 per cent. Since there are four moduli ratio curves, R is obtained for each curve by multiplying G^e by the factors 0.0013, 0.0016, 0.0020, and 0.0007, respectively; the values of H_0 for all the soils were taken to be equal to zero.

As in the Lotung case study, the parameters h and m also were determined for moduli ratio values of 0.9 and 0.5, along with Equation (6), and their profiles are shown in Figure 14. The zero-strain asymptotes of all the damping ratio curves indicate a viscous damping ratio of $\xi_0 = 3$

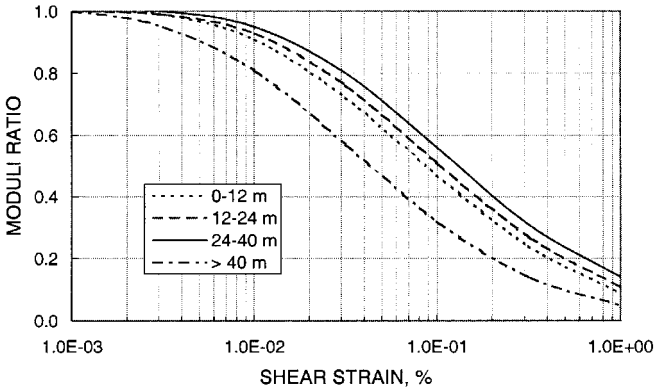

Figure 13. Moduli ratio curves for soil at Gilroy 2 site.

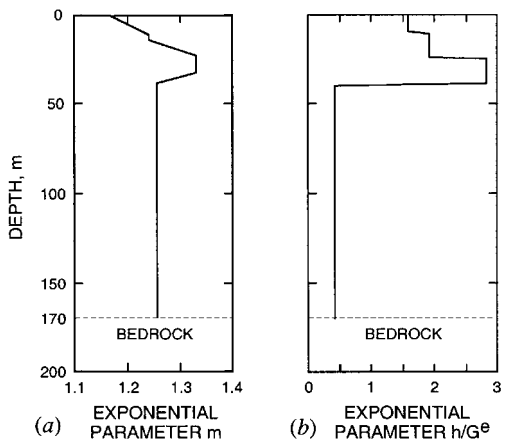

Figure 14. Exponential model parameters for soil at Gilroy 2 site: (a) exponent m; (b) coefficient h/G^e.

per cent at the Gilroy 2 site [20]. The dominant frequency at the rock site Gilroy 1 is around $f \approx 2.5$ Hz, while $f \approx 1.5$ Hz at Gilroy 2. It is expected that the overall representative dominant frequency over the soil layer at Gilroy 2 is somewhere between these two values, so we take $f \approx 2.0$ Hz. The choice of a representative f for the soil deposit is not crucial since the viscous damping ratio is only a small fraction of the total damping in the high-strain regime. From this, the material viscous damping parameter χ was estimated to be around 0.0048 s.

Figure 15 shows the modal responses of the stick FE mesh for the soil at Gilroy 2 site in the limit of elastic response. Here, we employ a mesh of 85 elements, each element having a thickness of 2 m, underlain by a bedrock at a depth of 170 m. Note that the low-frequency range is dominated by sway modes while the high-frequency range is dominated by vertical modes. For the sway and vertical modes the highest natural frequencies are about 130 and 385 Hz, respectively, which implies that the FE mesh is more than adequate to capture the frequency contents of the ground motion.

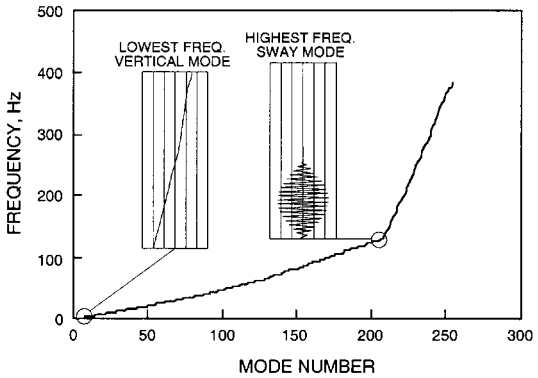

Figure 15. Frequency versus mode number for FE mesh: Gilroy 2 case study.

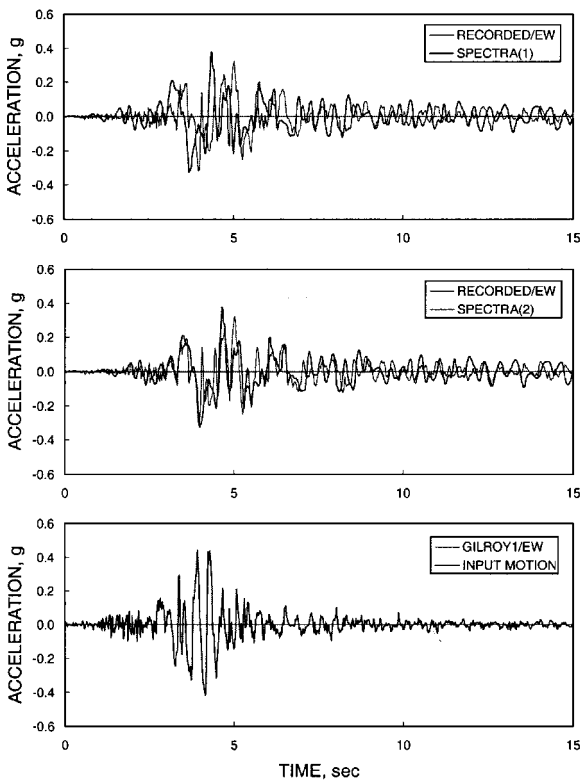

Figure 16. East–West acceleration-time history using SPECTRA: Gilroy 2 case study.

Figures 16 and 17 show the results of non-linear analysis in which the input motions at Gilroy 1 site are applied simultaneously at the Gilroy 2 bedrock site. 'SPECTRA(1)' pertains to solutions with no time shift, while 'SPECTRA(2)' pertains to solutions in which the times are shifted by 0.3 s so that the predicted peak ground acceleration coincides with the observed peak value. Recall

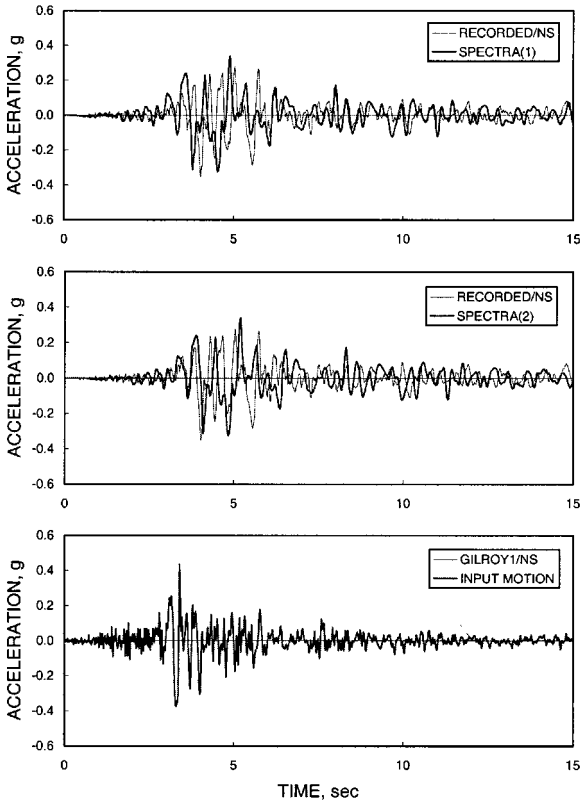

Figure 17. North–South acceleration-time history using SPECTRA: Gilroy 2 case study.

that the rock outcropping site Gilroy 1 is about 2 km away from the Gilroy 2 site, hence the expected delay in the arrival of the within rock motions at Gilroy 2 bedrock site. Note that the time-history plots with the times shifted agree better with the recorded responses. The predicted PGAs are 0.35*g* for the EW direction (recorded: 0.32 *g*) and 0.34 *g* for the NS motion (recorded: 0.35*g*). Qualitatively, the predictions shown in Figures 16 and 17 agree better with the recorded responses than those reported in Reference [20], as elaborated further in the next paragraph.

Figures 18 and 19 show the results of equivalent linear analyses using SHAKE for the Gilroy 2 case study. For comparison purposes, the predicted time histories have also been shifted by 0.3 s to account for the delay in the arrival of the input motion, and analyses were performed using both the 'within the soil profile' (WI) and 'rock outcropping' (OC) options to differentiate between total and free-field input motions. In general, the predicted responses are relatively unaffected by the choice of WI or OC options, except for the peak response in the NS direction where the peak response obtained with the WI option exceeds that obtained with the OC option by about 10 per cent. As shown in Figures 18 and 19, SHAKE overpredicted the peak values by about 50–100 per cent. Since SHAKE is an equivalent linear program, it is possible to differentiate between total and free-field motions because the principle of superposition holds. However, with a truly non-linear program like SPECTRA, where the soil response is assumed nonlinear everywhere, the

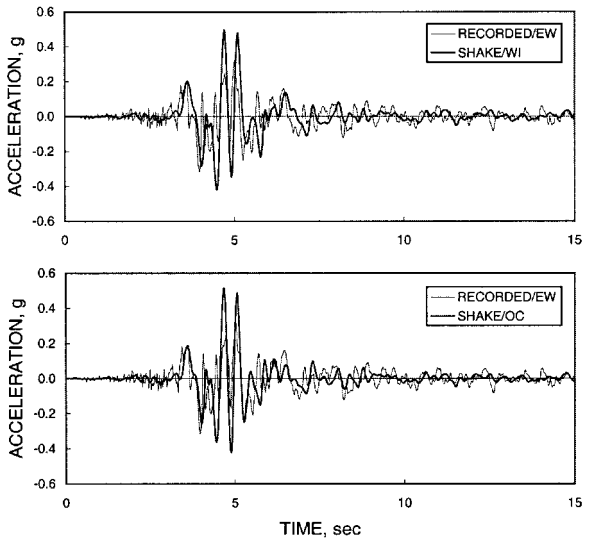

Figure 18. East–West acceleration-time history using SHAKE: Gilroy 2 case study. WI = 'within'; OC = 'outcropping'.

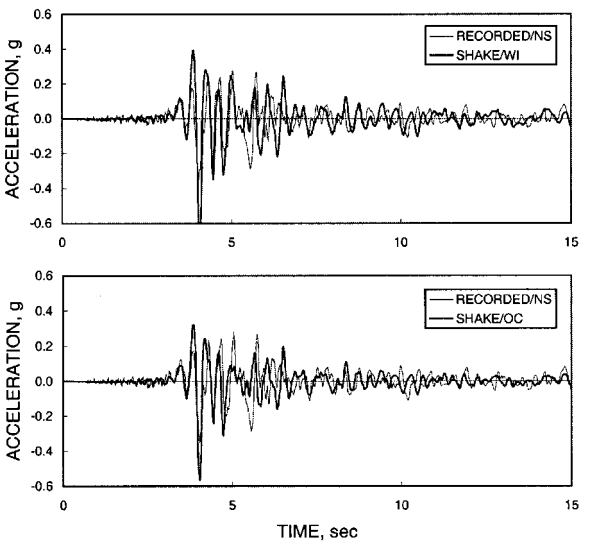

Figure 19. North–South acceleration-time history using SHAKE: Gilroy 2 case study. WI = 'within'; OC = 'outcropping'.

principle of superposition does not hold, and thus it is only possible to prescribe total input motions.

Finally, Figure 20 shows a maximum strain history plot for Gilroy 2 similar to Figure 11 for the Lotung case study. The plot of Figure 20 shows a permanent shear strain of 0.8 per cent, about

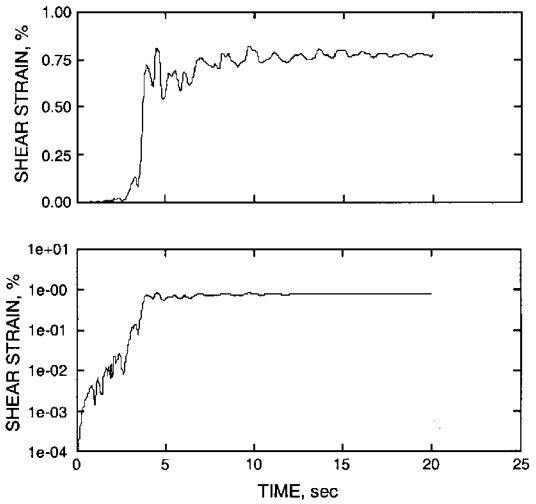

Figure 20. Normal and semi-logarithmic plots of time history of maximum shear strain developed in soil column for Gilroy 2 site response using SPECTRA.

five times larger than the permanent strain computed for the Lotung problem. As in the Lotung case study, most of these permanent deformations were observed to have accumulated during the period of strongest shaking, based on the results of the simulations. Separate sensitivity checks performed using different sets of model parameter values for R and H_0 (within the range implied by the moduli ratio curves reported in Reference [20]), suggest that the results of the Gilroy 2 simulations do not depend much on the values of R and H_0 either.

5. REMARKS ON NUMERICAL STABILITY

Stronger earthquakes were also studied to gain a better insight into the numerical stability of the proposed non-linear FE model in the regime of intense ground shaking. Included in these studies were hypothetical earthquakes derived from the LSST7 event of Section 3, but whose input motions were amplified by 2, 5, and 10 times. SPECTRA provided convergent results in all cases, while SHAKE failed to converge when the input motions were amplified by a factor of 5 or greater. This suggests better numerical stability of the non-linear model, as well as greater potential for application to cases involving larger earthquakes where equivalent linear analysis procedures typically have problems providing convergent solutions.

6. SUMMARY AND CONCLUSIONS

A model for nonlinear ground response analysis of non-liquefiable soils has been presented based on bounding surface plasticity with a vanishing elastic region. The formulation assumes general non-planar waves and couples all three kinematical components of motion. The model requires

less input information than SHAKE does, in that only the damping ratio value at near-zero shear strain is required, and not the entire damping ratio curve, and so the proposed model should be easier to use than SHAKE. The predictive capability of the model has been demonstrated from results of analyses of downhole motions recorded by an array at an LSST site in Lotung, Taiwan, and from the ground motion recorded at Gilroy 2 site. The general nature of the constitutive model facilitates a straightforward extension of the formulation to three-dimensional cases.

ACKNOWLEDGEMENTS

Financial support for this research was provided by the Earthquake Hazard Mitigation Division of National Science Foundation under Contract Nos. CMS-9114869 and CMS-9613906, through the program of Dr Clifford J. Astill. The writers would like to thank Dr H.T. Tang and Electric Power Research Institute for making the digitized data for the Lotung site available.

REFERENCES

1. Hardin BO, Drnevich VP. Shear modulus and damping in soils: design equations and curves. *Journal of Soil Mechanics and Foundations Division*, ASCE 1972; **98**:667–692.
2. Kramer SL. *Geotechnical Earthquake Engineering*. Prentice-Hall: Englewood Cliffs, NJ, 1996.
3. Seed HB, Idriss IM. Soil moduli and damping factors for dynamic analyses. *EERC Report No. 10-10*, Earthquake Engineering Research Center, University of California, Berkeley, CA, 1970.
4. Schnabel PB, Lysmer J, Seed HB. SHAKE—A computer program for earthquake response analysis of horizontally layered sites. *EERC Report No. 72-12*, Earthquake Engineering Research Center, University of California, Berkeley, CA, 1972.
5. Prevost JH. DYNA1D: A computer program for nonlinear site response analysis technical documentation. *Technical Report No. NCEER-89-0025,* National Center for Earthquake Engineering Research, SUNY at Buffalo, NY, 1989.
6. Martin PP, Seed HB. One-dimensional dynamic ground response analysis. *Journal of Geotechnical Engineering Division* ASCE 1982; **108**:935–952.
7. Streeter VL, Wylie EB, Richart FE Jr. Soil motion computations by characteristics method. *Journal of Geotechnical Engineering Division* ASCE 1974; **100**:247–263.
8. Borja RI, Amies AP. Multiaxial cyclic plasticity model for clays. *Journal of Geotechnical Engineering* ASCE 1994; **120**:1051–1070.
9. Dafalias YF, Popov EP. Cyclic loading for materials with a vanishing elastic region. *Nuclear Engineering and Design* 1977; **41**:293–302.
10. Zeghal M, Elgamal AW, Parra E. Identification and modeling of earthquake ground response—II. Site liquefaction. *Soil Dynamics and Earthquake Engineering* 1996; **15**:523–547.
11. Arulanandan K, Scott RF. (eds.), *Proceedings of the International Conference on Verification of Numerical Procedures for the Analysis of Soil Liquefac. Problems*, Vol. 2, Balkema, Rotterdam, 1994.
12. EPRI Report. Guidelines for determining design basis ground motions, Vol. 1: Method and guidelines for estimating earthquake ground motion in Eastern North America. Chapter 8: in *EPRI Technical Report No. TR-102293*, November 1993.
13. Borja RI, Chao HY, Montáns FJ, Lin CH. Nonlinear ground response at Lotung LSST site. *Journal of Geotechnical and Geoenvironmental Engineering*, ASCE 1999; **125**:187–197.
14. Borja RI, Chao HY, Montáns FJ, Lin CH. SSI effects on ground motion at Lotung LSST site. *Journal of Geotechnical and Geoenvironmental Engineering* ASCE 1999; **125**:760–770.
15. Hilber HM, Hughes TJR, Taylor RL. Improved numerical dissipation for time integration algorithms in structural dynamics. *Earthquake Engineering and Structural Dynamics* 1977; **5**:283–292.
16. Tang HT, Tang YK, Stepp JC. Lotung large-scale seismic experiment and soil-structure interaction method validation. *Nuclear Engineering and Design* 1990; **123**:197–412.

17. Anderson DG, Tang YK. Summary of soil characterization program for the Lotung large-scale seismic experiment, *Proceedings of the EPRI/NRC/TPC Workshop on Seismic Soil-Structure Interaction Analysis Techniques Using Data from Lotung, Taiwan* EPRI NP-6154, Vol. 1, 1989; 4.1–4.20.
18. Zeghal M, Elgamal AW, Tang HT, Stepp JC. Lotung downhole array. II: evaluation of soil nonlinear properties. *Journal of Geotechnical Engineering* ASCE 1995; **121**:363–378.
19. Chang CY, Mok CM, Power MS, Tang YK, Tang HT, Stepp JC. Equivalent linear and nonlinear ground response analyses at Lotung seismic experiment site. *Proceedings of Fourth U.S. National Conference on Earthquake Engineering*, Palm Springs, California, Vol. 1, 1990; 327–336.
20. EPRI Report. Guidelines for determining design basis ground motions, Vol. 2: Appendices for ground motion estimation. Appendix 6.B: in *EPRI Technical Report No. TR-102293*, November 1993.
21. Lee MKW, Finn WDL. *DESRA-2C*: *dynamic effective stress response analysis of soil deposits with energy transmitting boundary including assessment of liquefaction potential*. The University of British Columbia, Faculty of Applied Science, 1991.
22. Li XS, Wang ZL, Shen CK. *SUMDES*: *a nonlinear procedure for response analysis of horizontally-layered sites subjected to multi-directional earthquake loading*. Department of Civil Engineering, University of California, Davis, 1992.
23. Pyke RM. *TESS*: *a computer program for nonlinear ground response analyses*. TAGA Engineering Systems and Software, Lafayette, California, 1992.
24. Elgamal AW, Zeghal M, Parra E, Gunturi R, Tang HT, Stepp JC. Identification and modeling of earthquake ground response—I. Site amplification. *Soil Dynamics and Earthquake Engineering* 1996; **15**:499–522.
25. Li XS, Shen CK, Wang ZL. Fully coupled inelastic site response analysis for 1986 Lotung earthquake. *Journal of Geotechnical and Geoenvironmental Engineering* ASCE 1998; **124**:560–573.
26. Silva WJ. Global characteristics and site geometry. Chapter 6 in: *Proceedings*: *NSF/EPRI Workshop on Dynamic Soil Properties and Site Characterization*, EPRI Report No. NP-7337, Palo Alto, CA, 1991.

